scientific reports

OPEN

Design of a PIT biosensor based on plasmonic-graphene-black phosphorous hybrid for hypercholesterolemia detection

Esmat Rafiee

Cardiovascular diseases are the primary and fundamental reasons of people death around the world. Precise, fast responding, compact and integrable biosensors are considered as the most important prevention or treatment devices. In this work, remarkable absorbers based on graphene-plasmonic-black phosphorous hybrid structures are proposed. These devices are utilized for bio-sensing applications. The presented device is consisted of different quarter-cylindrical and plate shaped layers of graphene, black phosphorous, Ag, Au and Al_2O_3. In order to improve functionality of the presented absorber (improving the absorption's peak value), effects of structural parameters and chemical potential (E_f) on the absorption spectrum are being considered. The proposed structure will be considered as a biosensor for detection of cholesterol concentrations in blood samples (this would help physicians in diagnosis of hypercholesterolemia and prevention of cardiovascular diseases), after improving its characteristics. Finally, it is expected for this biosensor the following remarkable sensitivity, figure of merit, quality factor and detection limit of 6045.6 nm/RIU, 237.61 RIU^{-1}, (80.3–90.1) and (2.1e-4–2.26e-5) RIU, respectively. Therefore, the proposed device can be an appropriate candidate for bio-sensing applications in optical integrated circuits.

Keywords Bio-sensor, Black phosphorous, Cardiovascular diseases, Hypercholesterolemia, PIT, Plasmonic-graphene

According to world health organization (WHO), cardiovascular diseases (CVDs) are the primary and main reasons of people death in the world (causing death of 17.9 million people each year). As known, CVDs are categories of heart and blood vessels mal-functionalities which generally lead to heart attacks and strokes. Hypercholesterolemia is mostly the main reason of severe heart diseases. Therefore, detection of cholesterol and its high levels (hypercholesterolemia) in early stages and with high precisions can fundamentally help physicians and patients (prevention of heart diseases; decreasing chance of suffering heart attacks and strokes). Due to the vitality of cholesterol diagnosis for scientists, various detection methods and devices were proposed and designed over the years. The proposed systems (biosensors) were considered based on various operation principles like electrochemical[1,2], piezoelectric[3], optical[4–7] and etc. Among the mentioned operation principles, optical ones have attracted remarkable attentions due to their higher precision, accuracy, response time, sensitivity and lower cost and dimension[8,9]. Optical based biosensors have been extensively considered and investigated[10]. They are particularly utilized for sensing applications[10]. Optical biosensors can be fabricated considering hybrid configurations. A photonic crystal-based biosensor was suggested for detection of glucose in blood samples with remarkable sensitivity of 4200 nm/RIU[11]. Combination of bimetallic-MXene-graphene was considered for rapid diagnosis of malaria with appropriate sensitivity[12]. In another research[13], Ag-graphene-prism-perovskites combinations were considered for diagnosis of basel cancerous cells. Considerable sensitivity of 298.5 deg/RIU was obtained[13]. In another work[14], plasmodium falciparum infections could be detected considering Ag-$BiFeO_3$-graphene-MXene-phosphorene nano combination. The structure functioned based on SPR effect with acceptable sensitivity of 461.43 deg/RIU[14].

Plasmonic-graphene-black phosphorous (BP) combination can be an appropriate candidate for precise bio-sensing applications. Plasmonic nano structures can be designed based on different dielectric and metal layers[15] while graphene structures can be configured based on 2-D lattices of carbon atoms[16]. Black phosphorous nano structure is consisted of a 2-D semiconductor which has the same dimension as graphene (while acquiring

Department of Electrical Engineering, Faculty of Engineering, Alzahra university, Tehran, Iran. email: e.rafiee@alzahra.ac.ir

higher scalability and integrability compared with graphene)[17,18]. A monolayer of black phosphorous known as a phosphorene (which has a direct bandgap from 0.3ev (for phosphorene) to 2ev (for bulk BP)) is considered for designation process[19,20]. Plasmonic-graphene-BP hybrid structure can interestingly scale down the dimension, proposing an appropriate configuration for optical integrated circuits (with dimensions lower than the incident wavelength). As known, fabrication process of nano-dimension structures like graphene, plasmonic, BP or their combinations is challenging and complicated. However, some techniques like electron-beam lithography, focused-ion lithography, dip-pen lithography, laser interference lithography, nano-sphere lithography and etc., can be considered for implementing graphene-plasmonic-phosphorene hybrid structures[21–24].

Surface plasmon resonance (SPR) effect is the basic application principle of the plasmonic-graphene-BP hybrid system. In SPR effect, surface plasmon polaritons show stronger field energies near the interfaces (between two media) which can effectively improve functionality of the proposed biosensor (sensitivity of the suggested device can be improved, in fact different sensing medium considered by their refractive indices (RIs) can be precisely detected)[25–27]. A ZnO layer combined with CaF_2 prism operating based on SPR effect was considered for detection of SARA-CoV-2[28]. Notable sensitivity of 364.17o/RIU was obtained for the proposed biosensor[28]. As known, hybrid structures functioning based on plasmon induced transparency (PIT) effects have been of great interest to researchers in recent years. In these devices, a transparent window in the absorption spectrum (low absorption amount or high transmission amount), can be utilized for various applications like switching[29,30], sensing[31,32], logical functioning[33] and etc. Actually, in SPR based devices, quantum interference of two paths can induce PIT window in the absorption diagram[34]. Increased dispersion and high slow light effect in the PIT window (near zero absorption value) can help design biosensors with remarkable sensitivity factors[31]. Hybrid plasmonic-graphene-BP structure effectively takes advantage of the ability of exciting PIT in the NIR range (by BP structure)[35], resonance wavelength tunability and high EM field intensity (by considering plasmonic-graphene combination)[36,37]. As a result, considering PIT effect in the plasmonic-graphene-BP hybrid structure can increase the biosensor's sensitivity and improve its functionality[38,39].

As stated, high cholesterol concentrations can cause hypercholesterolemia which might lead to heart attack and strokes. Thus, proposing non-invasive techniques for early, fast and precise detection of cholesterol concentration in blood samples are important. In recent years, many researchers have focused their works on proposing optical biosensors for detection of biological elements; especially cholesterol. In[40], an SPR optical fiber biosensor based on Au layers and nanoparticles was proposed. The structure was utilized for detection of glucose and cholesterol with acceptable detection limit. In another research[1], multimode fiber and hollow fiber structures were considered for detection of cholesterol concentration. Appropriate detection limit and sensitivity factor were obtained for the proposed biosensor. In[7], a dual mode cholesterol biosensor was proposed which was based on gold rods and carbon quantum dots. For the proposed structure, detection limit of 0.028μM was obtained. Also in[41], an Organometal lead halide perovskites photo-electrochemical biosensor for detection of cholesterol concertation was presented. The structure was considered with water stability and indicated acceptable results. In another structure[42], by considering Cyclodextrin capping gold nanoclusters fluorescent probes, a cholesterol detection biosensor with high sensitivity was proposed. Wide linear response range (20.00 ~ 150.00 $\mu mol \cdot L^{-1}$) and appropriate detection limit (16.07 $\mu mol \cdot L^{-1}$) were the advantages of the designed biosensor. In[43], a photonic crystal fiber biosensor based on octagonal hollow core-shaped structure was suggested. The proposed structure was considered for detection of cholesterol concentrations in blood samples with low confinement loss of $3.14 \times 10^{-20}\ cm^{-1}$ and low effective material loss of 0.0008 cm^{-1}. Recently[44], by considering graphene oxide, zinc oxide and etc., a sensitive biosensor for detection of cholesterol and bilirubin was proposed. Sensitivity factors of 0.92 $\mu A\ \mu M^{-1}\ cm^{-2}$ and 0.2 $\mu A\ \mu M^{-1}\ cm^{-2}$ were obtained for cholesterol and bilirubin concentrations, respectively.

In this research, a biosensor for detection of cholesterol concentration in blood samples is proposed. Fast and precise detection of cholesterol concentrations can prevent cardiovascular diseases and strokes. The presented system is a hybrid of the graphene-plasmonic-BP nano combination which function based on the PIT effect (double peaks). Remarkable sensitivity, figure of merit and quality factor are the main advantages of the proposed biosensor.

Proposed structure and theoretical model

The first designed plasmonic-graphene-BP absorber is presented in Fig. 1.

The first presented system is consisted of two quarter-cylindrical shaped waveguides (in which the arches are made of graphene and other surfaces are consisted of phosphorene) and a plate-shaped gold (Au) layer which are situated in a substrate of Al_2O_3. The plate shaped layer of silver (Ag) (which is positioned in the bottom of the structure) acts as a mirror which facilitates concertation of light wave in the structure. Therefore (by considering Ag layer as a mirror), absorption peak can be effectively improved (even creating a perfect absorber)[31,32]. Geometrical parameters of the proposed absorber are stated in Table 1.

Numerical simulations were considered by utilizing 2-D finite element (FE) software (COMSOL Multiphysics 5.5).

In order to study the absorption properties of the designed system, following relation can be investigated[45,46]:

$$A(\omega) = 1 - R(\omega) \tag{1}$$

According to Eq. (1), for having a perfect absorber ($A(\omega) = 1$), $R(\omega)$ should be zero. In this case, the light wave would be perfectly absorbed in the structure. In order to study the properties of the presented structure, specifications of each layer (graphene, Ag, Au and BP) should be investigated. For the graphene layers, surface conductivity parameter can be considered by studying Kubo formula[45,47]:

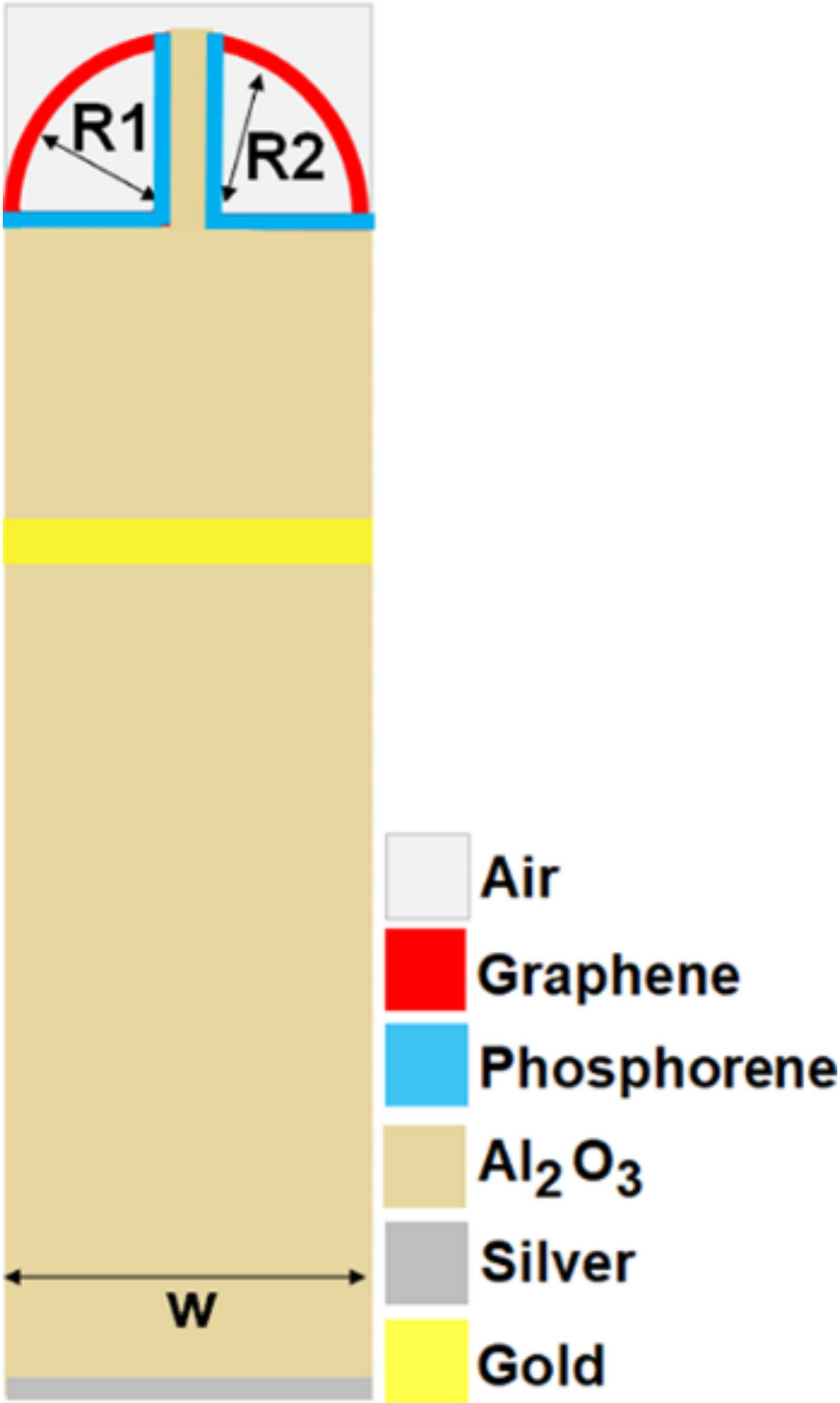

Fig. 1. Schematic of the first designed plasmonic-graphene-phosphorene absorber.

$$\sigma_g(\omega, E_f, \Gamma, T) = \sigma_{g-real} + j\sigma_{g-imag} = \sigma_{\text{int}\,ral} + \sigma_{\text{int}\,er} \tag{2}$$

where ω, E_f, Γ and T represent the operation frequency, chemical potential, phenomenological scattering rate and absolute temperature, respectively. For the graphene layer, intra- and inter-band electro-photon scattering factors can be stated as[45,47]:

Parameter	Value (nm)
W	525
R_1	250
R_2	250
R_3	250
R_4	250
R_5	250
R_6	250
R_7	250
R_8	250
$h_1 = h_2$	80
t_1	25
t_2	25
t_3	10
M	100

Table 1. Geometrical parameters of the proposed absorber.

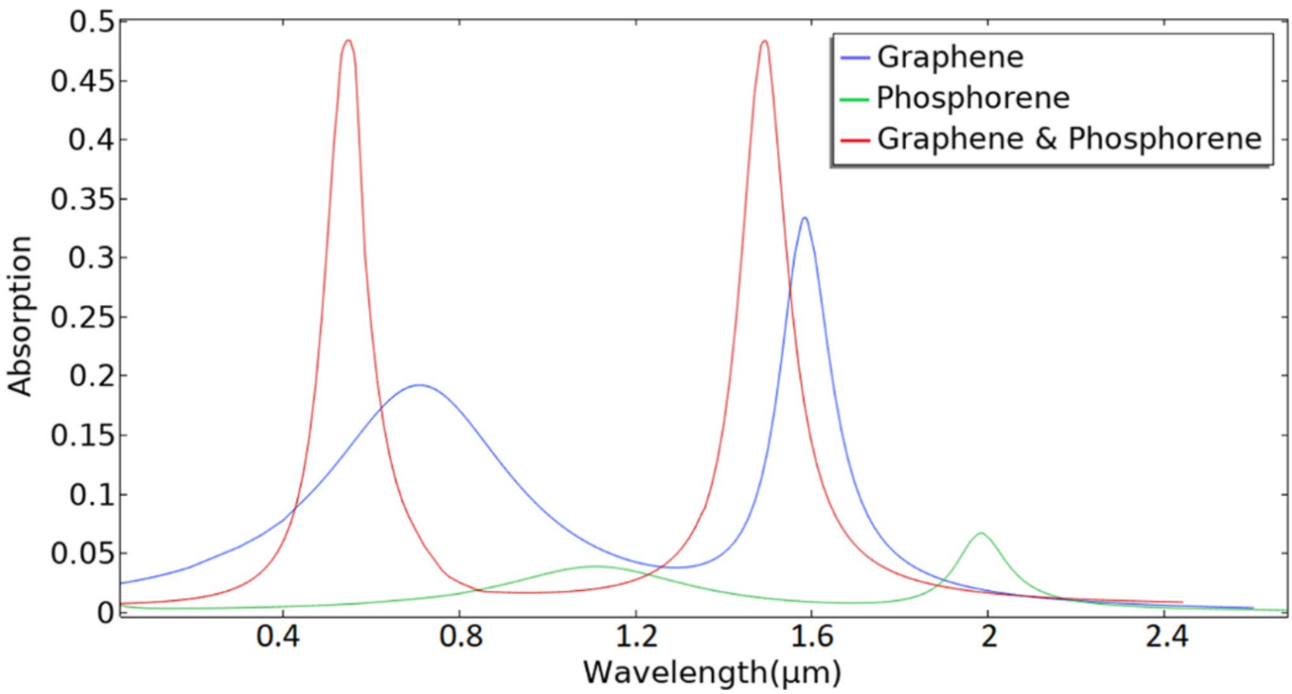

Fig. 2. View of the absorption spectrum for three cases.

$$\sigma_{\mathrm{int}\,ra} = -j\frac{e^2 k_B T}{\pi\hbar^2\left(\omega - j2\Gamma\right)} \times \left[\frac{E_f}{k_B T} + 2\ln\left(\exp\left(-\frac{E_f}{k_B T}\right) + 1\right)\right] \tag{3}$$

$$\sigma_{\mathrm{inter}} = -j\frac{e^2}{4\pi\hbar}\ln\left[\frac{2\left|E_f\right| - \left(\omega - j2\Gamma\right)\hbar}{2\left|E_f\right| + \left(\omega - j2\Gamma\right)\hbar}\right] \tag{4}$$

where k_B, T and e stand for the Boltzmann constant, temperature and electron charge, respectively.

For the Au and Ag layers, Drude model can be utilized for studying the dielectric function[48]:

$$\varepsilon\left(\omega\right) = \varepsilon_\infty - \frac{\omega_p^2}{\omega^2 + i\omega\gamma} \tag{5}$$

where $\varepsilon_\infty = 3.7$ (dielectric constant at infinite frequency), $\gamma = 0.018$ eV (collision plasma angular frequency) and $\omega_p = 9.1$ eV (bulk plasma angular frequency)[48].

Specifications of the single BP layer (phosphorene) can be studied by utilizing the conductivity ($\sigma_{x,\ y}$) formula[31,49]:

$$\varepsilon(\omega) = \varepsilon_{\infty} - \frac{\omega_p^2}{\omega^2 + i\omega\gamma} \tag{6}$$

where $\sigma_{x,\ y}$ (armchair and zigzag direction conductivities of BP), $\eta = 10\ meV$ (scattering rate), $D_n = \pi e^2 n/m_n$ (Drude weight) and n (carrier density of phosphorene).

In the following sections, for investigating the functionality of the designed structure (presented in Fig. 1), its absorption spectrum will be obtained. After that, other layers of graphene and phosphorene will be added for improving the absorption's peak value. In other steps, effects of different structural parameters and chemical potential of the graphene layer will be considered (for increasing the absorption's peak value). Finally, the improved designed system will be considered as a biosensor for detection of cholesterol concentrations in blood samples.

Results and discussion

In this section, the structure presented in Fig. 1 will be considered. First, the absorption diagram for three conditions is investigated (structure with a phosphorene layer, structure with a graphene layer and structure with both phosphorene and graphene layers).

As seen in Fig. 2, best absorption spectrum is obtained for the third case (structure with both phosphorene and graphene layers). As known, plasmon induced transparency (PIT) effect can be happened through the bright and dark mode's coupling[20,50]. Input signal can excite the bright mode, while it can't excite the dark mode (dark mode is independent of the external conditions). Phosphorene and graphene-based systems can excite the bright and dark modes, respectively[31]. PIT effect can be occurred through the interaction of the phosphorene-graphene hybrid system. Therefore, combination of the phosphorene and graphene nano structures will be considered and designed. In the following section, the second hybrid structure (containing two more quarter-cylindrical shaped waveguides; for improving the absorption spectrum) is presented.

S proposed graphene-plasmonic-phosphorene hybrid structure

The second designed absorber (with two added phosphorene and graphene quarter-cylindrical shaped waveguides) is presented in Fig. 3.

In Fig. 4, absorption diagram (considering two cases; adding only one quarter ring (R_3) and adding both (R_3 and R_4)) is depicted.

As seen in Fig. 3, by adding R_3 and R_4, an approximate ring covered by graphene will be formed. According to the following equation, resonant wavelength is proportional to ring circumference (radius) (λ is proportional to L).

$$nL = m\lambda \tag{7}$$

where n, m, $L = 2\pi r$, r and λ represent the refractive index of the ring resonator, integer value, circumference of the ring resonator, ring radius and resonant wavelength of the ring resonator, respectively[51]. Therefore, when a complete ring is formed (by adding R_3 and R_4), circumference of the ring would be increased (higher ring radius). This would lead to the increment of the resonant wavelength (red-shift). It can also be concluded from Fig. 4, that adding two more quarter-cylindrical shaped waveguides (with radii of R_3 and R_4) will lead to better results. As seen in Fig. 4, third case (containing both R_3 and R_4) indicates higher absorption peaks compared with adding only R_3. As the absorption's peak value is not yet satisfying (Fig. 4), third structure would be proposed and then would be improved considering its structural parameters.

Third proposed graphene-plasmonic-phosphorene hybrid structure

The third designed absorber (with four added phosphorene and graphene quarter-cylindrical shaped waveguides under the Au layer) and its 3-D view are presented in Fig. 5.

In this part, absorption diagram for the third proposed structure will be extracted. Figure 6 shows the absorption spectrum (considering adding four individual phosphorene and graphene quarter-cylindrical shaped waveguides in four steps; first adding R_5, then adding R_6, after that adding R_7 and finally adding R_8). As can be seen, by adding extra graphene and phosphorene layers, incident light wave will be better absorbed which would improve characteristics of the presented structure.

As seen in Fig. 6, best absorption spectrum with the peak of ~ 0.74 is obtained for the case of adding R_5, R_6, R_7 and R_8. Although, the absorption's peak value is considerably improved compared with the first proposed structure, it is not yet appropriate for bio-sensing applications. Therefore, in the following sections, effects of structural parameters and chemical potential will be investigated (for improving the absorption's peak value).

Investigating the effects of "E_f"

In this section, effects of "E_f" (chemical potential) on the absorption diagram are investigated and the result are depicted in Fig. 7.

As shown in Fig. 7, increasing "E_f" from 0.3 ev to 0.9 ev would shift the absorption's peak value to higher amounts (from 0.74 to 0.8 for the left and right peaks). These variations can be explained by the circuit theory. In the circuit theory, graphene can be defined as a shunt admittance which will be varied by the structural parameters and chemical potential E_f. As a result, graphene can be substituted by resistors, capacitors and inductors. Thus, altering E_f can vary the absorption's peak wavelength according to the following Eqs[4,9,34].

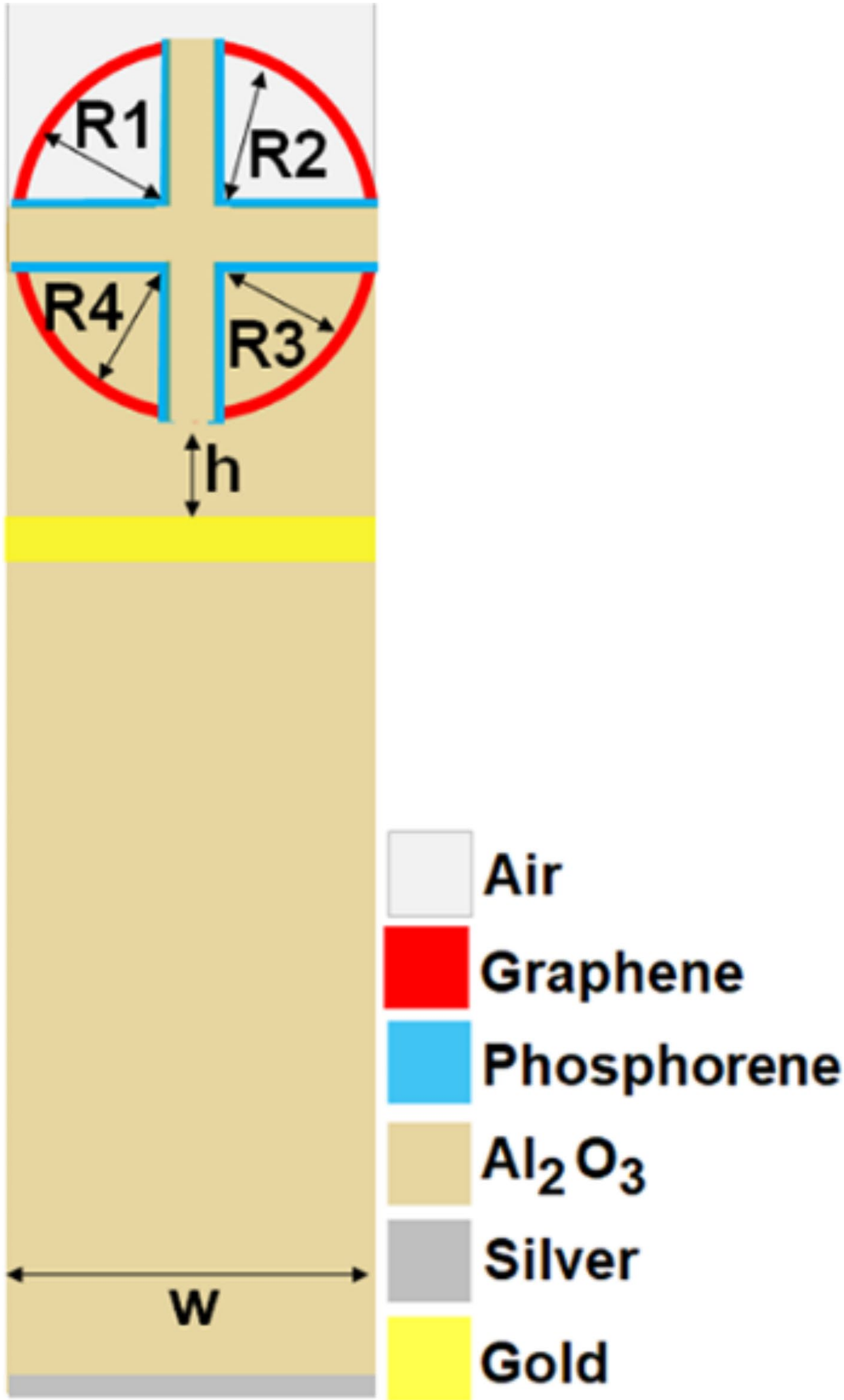

Fig. 3. Schematic of the second proposed absorber.

$$\varepsilon(\omega) = \varepsilon_\infty - \frac{\omega_p^2}{\omega^2 + i\omega\gamma} \tag{8}$$

where *c*, *L* and *C* stand for the speed of light in vacuum, capacitance and inductance of the circuit, respectively. It can be concluded that increasing E_f would decrease *L*, which would shift the absorption's peak wavelength to lower amounts (blue shift) (this occurs for the right peaks of Fig. 7).

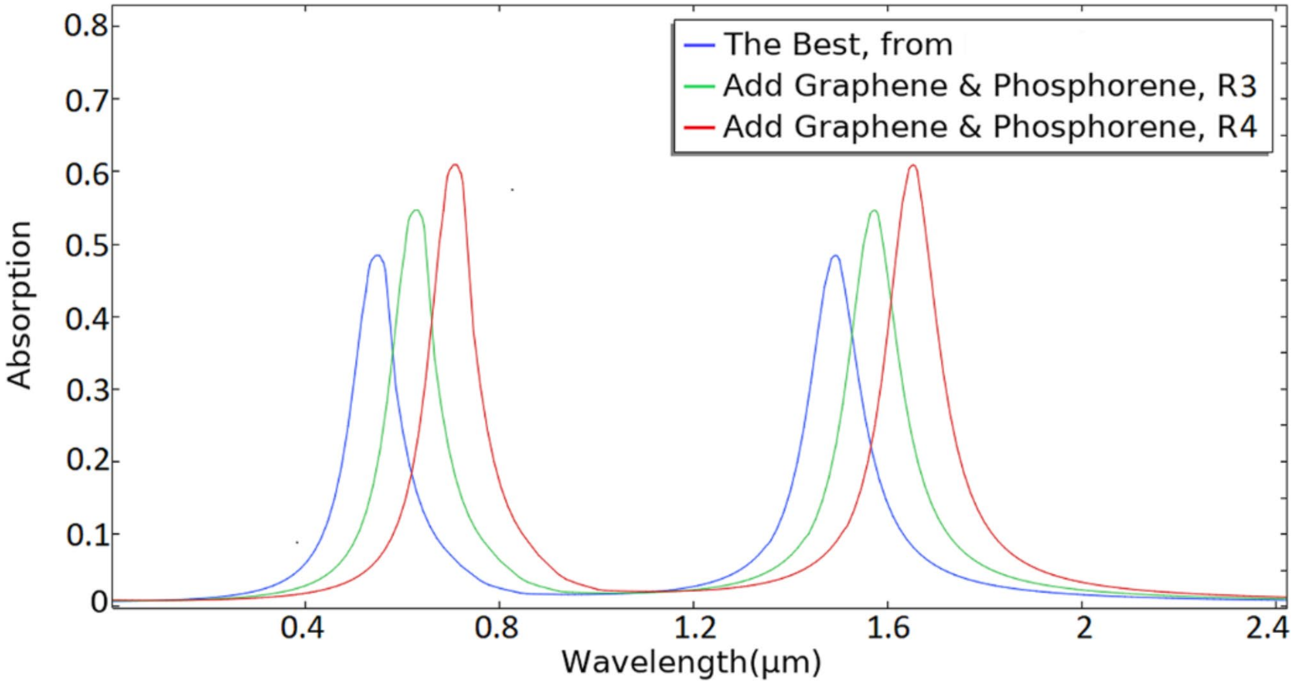

Fig. 4. View of the absorption spectrum for two conditions.

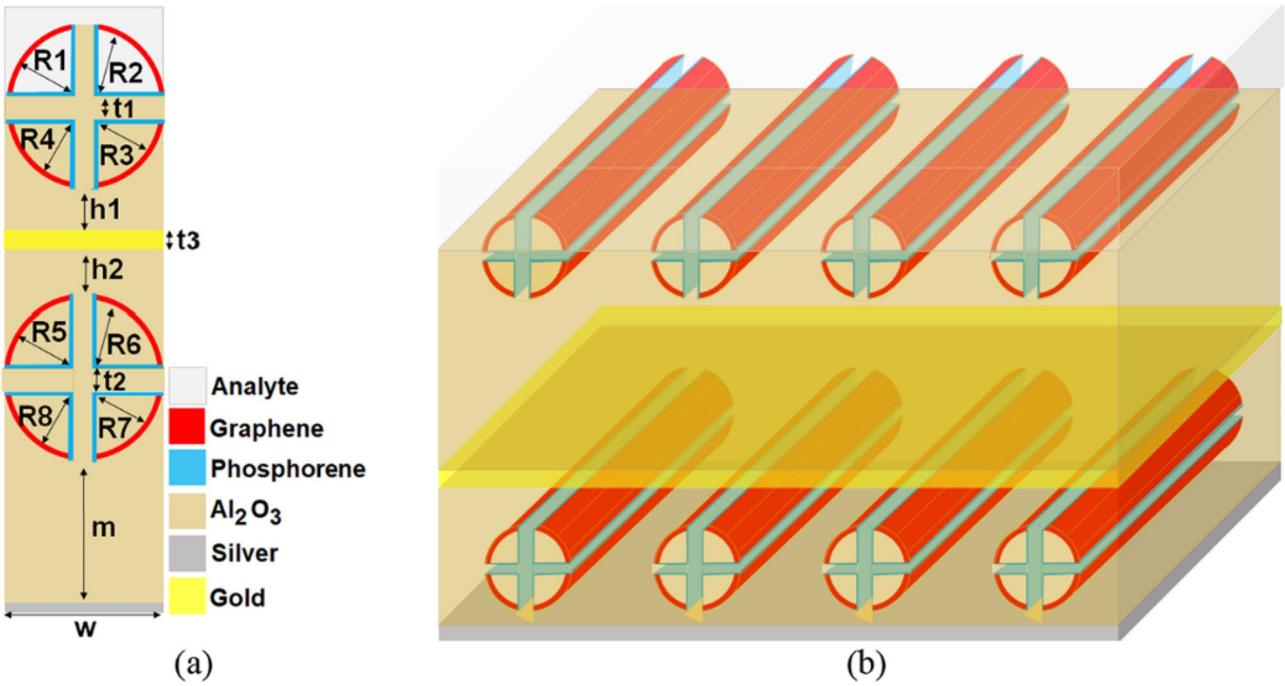

Fig. 5. (a) View of the third designed system (b) 3-D view of the third designed system.

Finally, best value of $E_f = 0.9$ ev is considered for the following parts. In the following part, effects of quarter-cylindrical shaped waveguide's radii (R_1, R_2, …and R_8) will be investigated. For ease of fabrication, analysis and simulation, all of the quarter-cylindrical shaped waveguide's radii will be considered the same ($R_1 = R_2$, … $= R_8 = R$).

Considering the effects of "R"

In this part, effects of quarter-cylindrical shaped waveguide's radii on the absorption spectrum is considered and shown in Fig. 8.

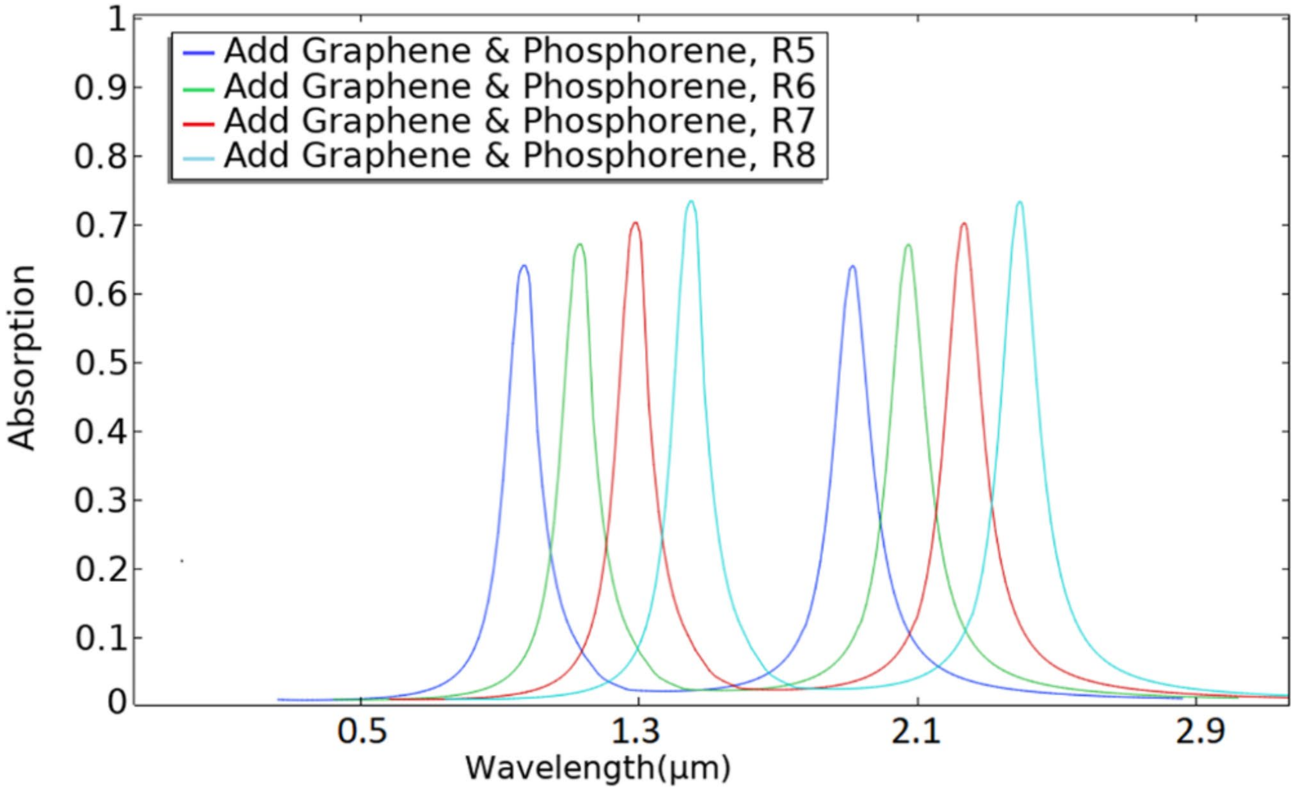

Fig. 6. Schematic of the absorption spectrum for the four cases (first adding R_5, then adding R_6, after that adding R_7 and finally adding R_8).

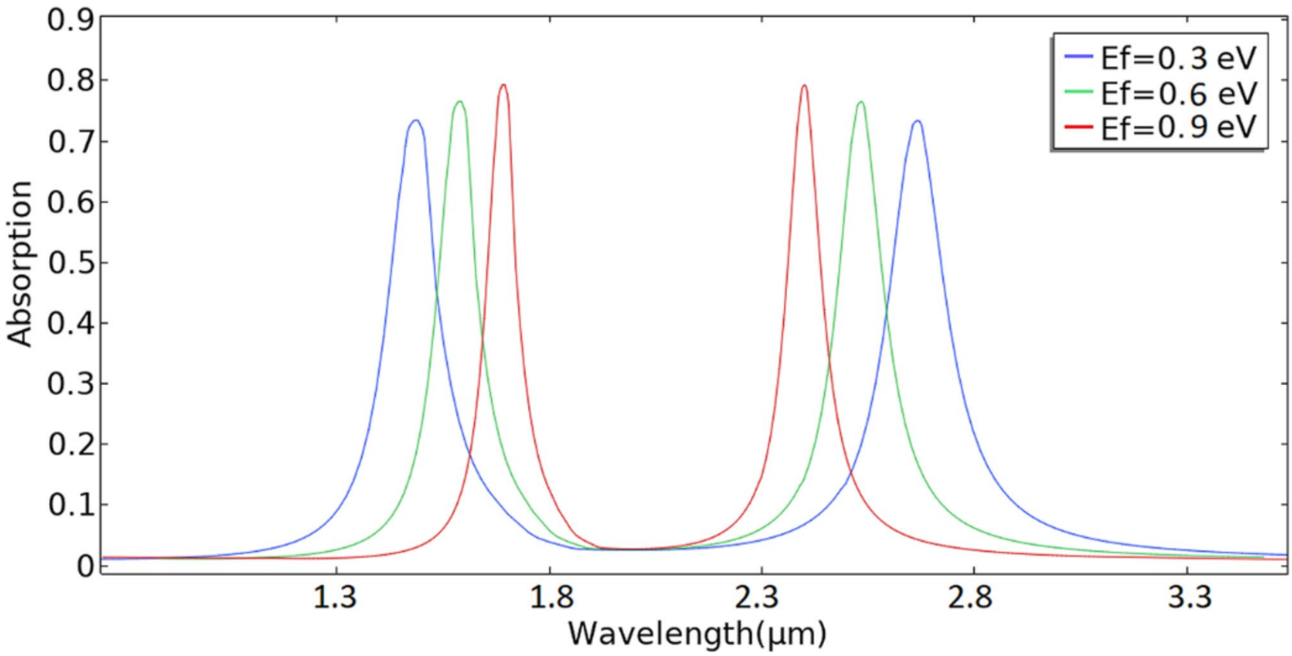

Fig. 7. View of the absorption spectrum versus wavelength for different values of "E_f".

As shown in Fig. 8, by altering R from 150 nm to 350 nm, absorption's peak value will be shifted from 0.2 to 0.88 (the left peak) and from 0.34 to 0.88 (for the right peak). It can be seen that absorption's peak wavelength is red-shifted (moves to higher wavelengths). This phenomenon can be explained by Eq. (7). As can be concluded from Eq. (7), increasing "R" will also increase L. According to Eq. (7), increasing L will also enhance λ (shift λ

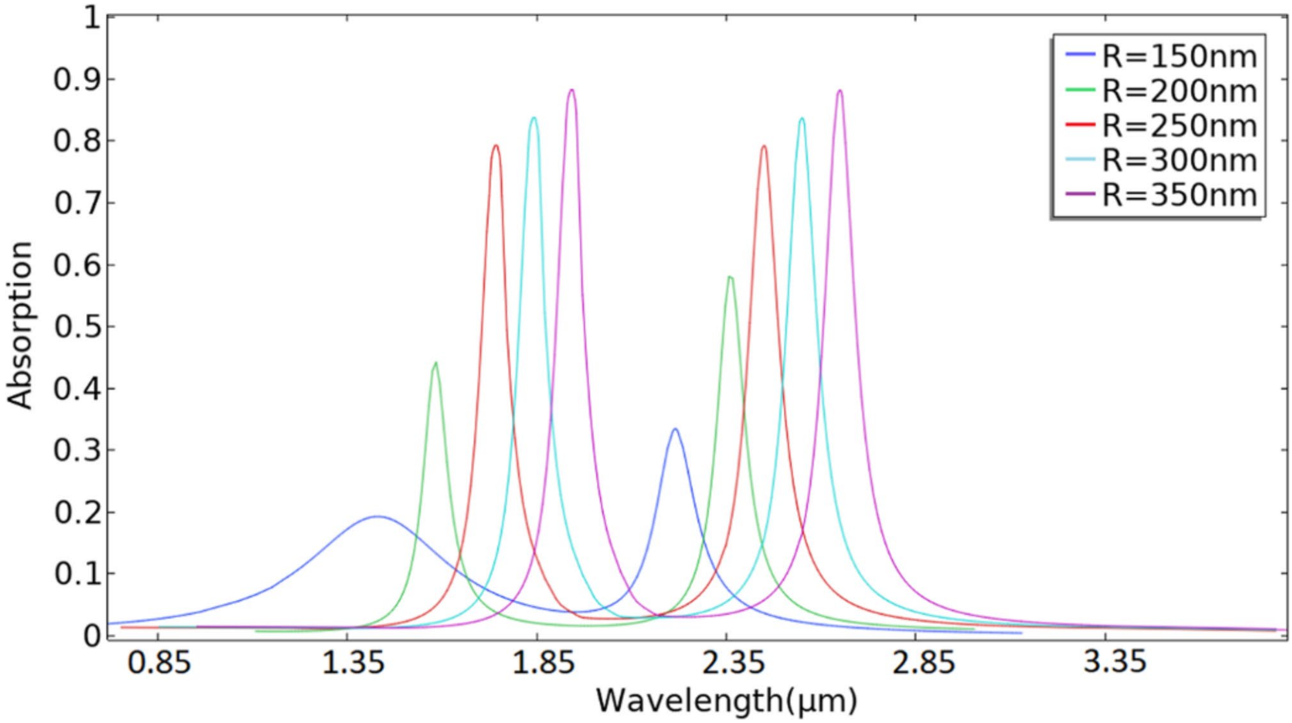

Fig. 8. Schematic of the absorption spectrum versus wavelength for different values of "*R*".

"resonant wavelength" to higher values). Therefore, enhancing radius will increase the resonant peak wavelength. As seen in Fig. 8, increasing *R* will enhance the absorption's peak value. This phenomenon occurs due to the enhanced confinement of the signal in the phosphorene and graphene structures.

Finally, best result is obtained for $R = 350$ nm with the resonant peak value and wavelength of (0.88, 1.93 μm) for the left peak and (0.88, 2.7 μm) for the right peak, respectively. For the following studies, $R = 350$ nm will be considered.

Investigating the effects of "t_1 and t_2"

In this part, effects of "t_1 and t_2" (coupling distance between the four upper and lower quarter-cylindrical shaped waveguides) on the absorption diagram are investigated and shown in Fig. 9. For ease of fabrication, analysis and simulation, "$t_1 = t_2$" is considered.

As shown in Fig. 9, coupling distance "t_1 and t_2" between neighboring quarter-cylindrical shaped waveguides can affect absorption spectrum. In fact, by adjusting this parameter, PIT coupling strength can be varied[34]. As seen, by increasing "t_1 and t_2", resonant peak will be enhanced while PIT window would be shrink. Finally, best resonant peak value and wavelength of (0.93, 1.95 μm) for the left peak and (0.93, 2.52 μm) for the right peak are achieved, respectively. For the following studies, $t_1 = t_2 = 45$ nm will be considered.

Considering the effects of "$h_1 + h_2$"

In this section, effects of "$h_1 + h_2$" (shown in Fig. 5) on the absorption spectrum will be studied and shown in Fig. 10.

As shown in Fig. 10, coupling distance "$h_1 + h_2$" between the upper and lower four quarter-cylindrical shaped waveguides can affect absorption spectrum. Variation processes of "$h_1 + h_2$" are the same as that of "t_1 and t_2". Therefore, by enhancing "$h_1 + h_2$", resonant peak will be increased and PIT window dimension will be decreased. In order to investigate functionality of the proposed structure, field distribution at various wavelengths "a, b, c" shown in Fig. 10 will be considered in the following section.

Field distribution spectrum for three individual wavelengths shown in Fig. 10

In this section, electric field distribution diagrams (for two peaks and a dip) (wavelength of the induced transparent window) of Fig. 10 are extracted and shown in Fig. 11.

Electric field distribution diagram of three wavelengths ("$\lambda = 2.05$μm and $\lambda = 2.5$μm" peak wavelengths of the absorption diagram, "$\lambda = 2.2$μm" dip wavelength of the absorption diagram) are shown in Fig. 11. As can be seen, wavelength of "b" is positioned in the PIT window.

Presented graphene-plasmonic-phosphorene hybrid Biosensor for cholesterol detection

In this section, different concentrations of cholesterol with various RIs are considered as biological elements in the Analyte section of Fig. 5. The presented biosensor is considered to operate based on the plasmon-induced transparency (PIT) effect. In the bio-sensing application, analyte would be inserted in the upper layer while

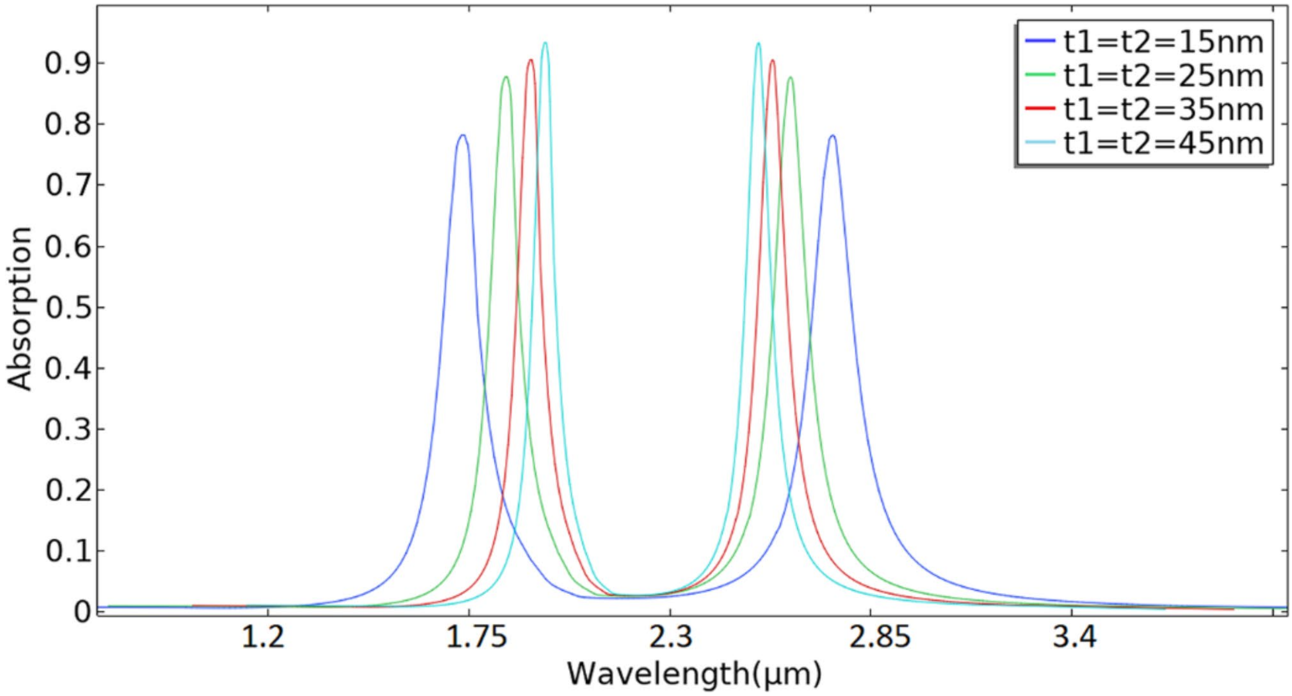

Fig. 9. View of the absorption spectrum versus wavelength for different values of "t_1 and t_2".

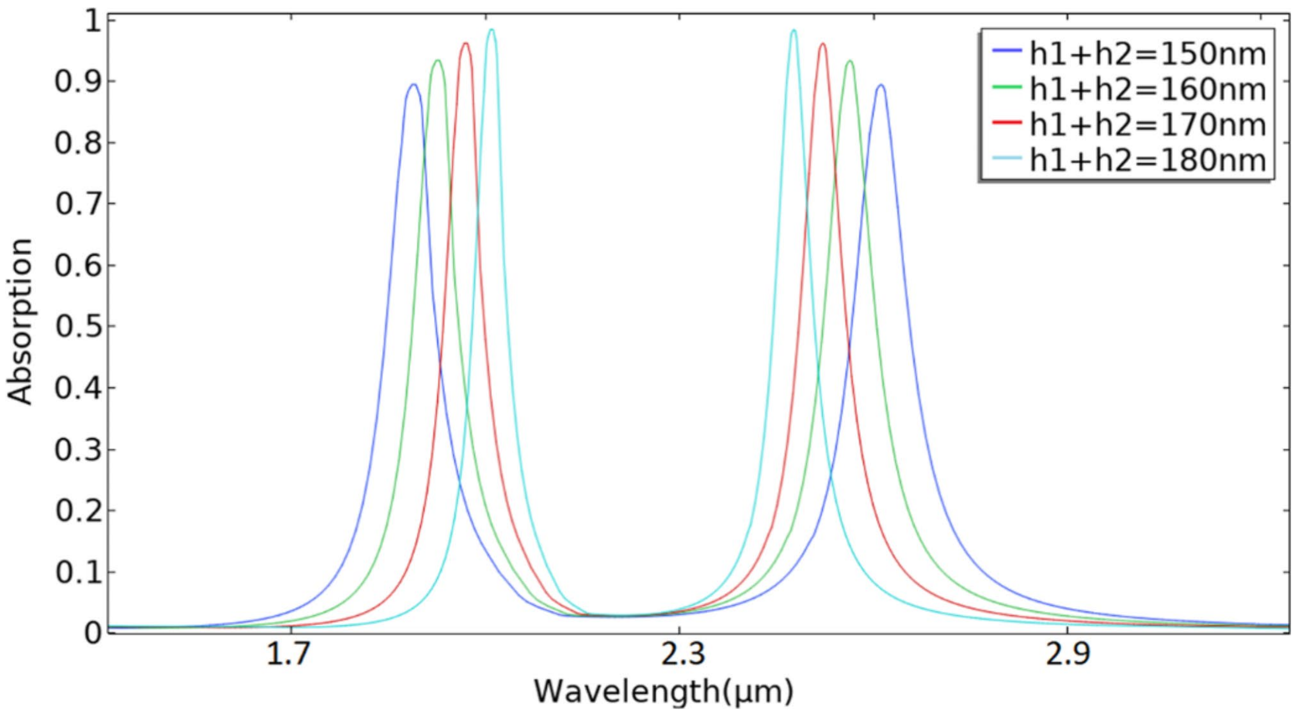

Fig. 10. Schematic of the absorption spectrum versus wavelength for different values of "$h_1 + h_2$".

being in contact with the incident light wave. Absorption spectrum consisting PIT window would be achieved; in which different concentrations of cholesterol defined by their refractive indices (RIs) can be detected. Absorption diagram is shown in Fig. 12.

The refractive indices considered in Fig. 12 as 1.48, 1.485, 1.49 and 1.495 are related to various cholesterol concentrations in blood samples ($n = 1.48$ for 0.01%, $n = 1.485$ for 0.06%, $n = 1.49$ for 0.09% and $n = 1.495$ for 0.13%[52]). As can be seen in Fig. 12, enhancing RI will increase the absorption peak wavelength[9,24,53].

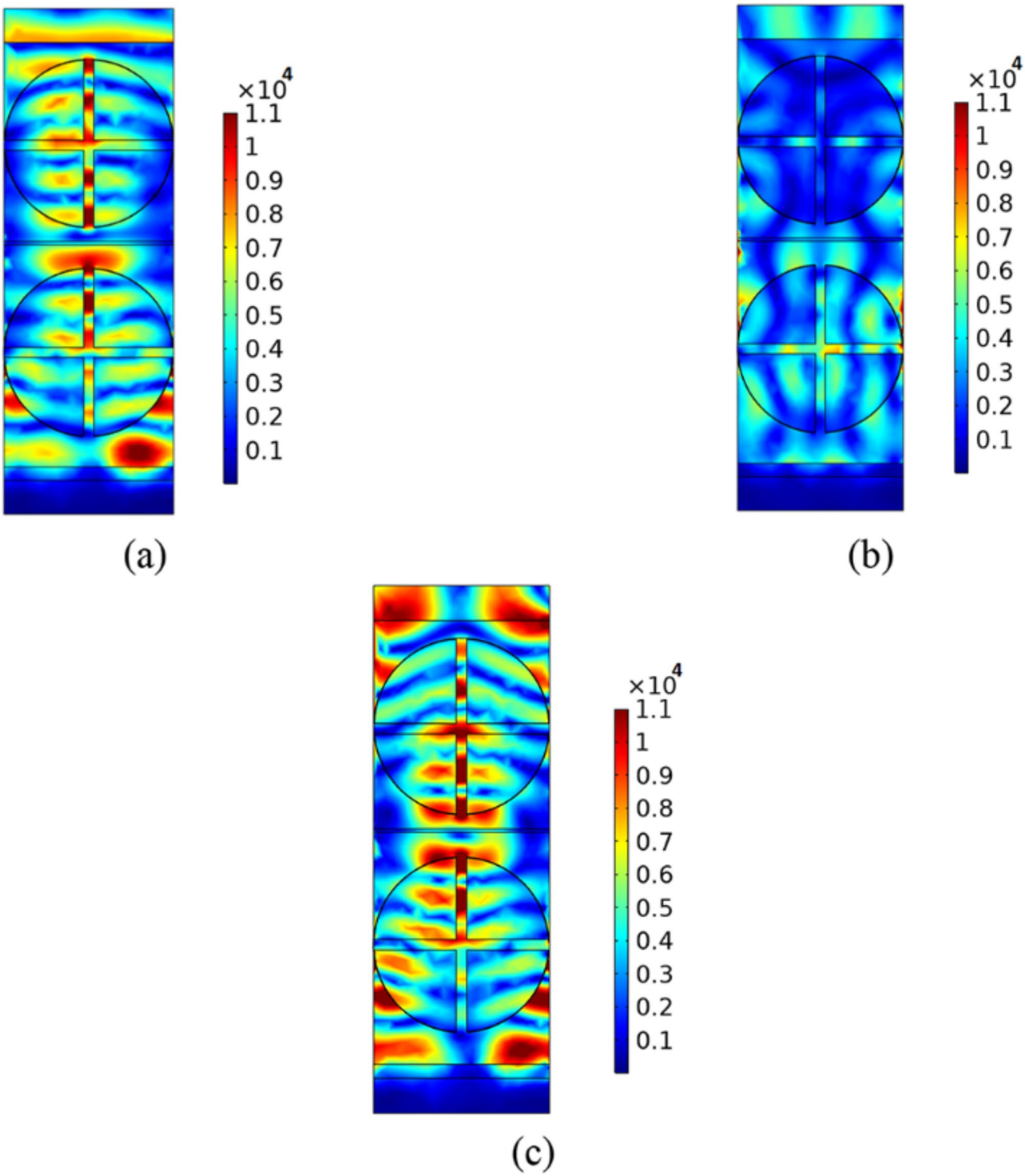

Fig. 11. Field distribution diagram related to the absorption spectrum (Fig. 10) for (a) point "a", (b) point "b" and (c) point "c".

Considering the results obtained from this biosensor, physicians can diagnose hypercholesterolemia in early stages (preventing cardiovascular diseases and heart attacks and strokes).

Some important factors which can describe the functionality of the proposed biosensor will be stated in the following part. Sensitivity factor is one of the most important factors which can be obtained according to the following equation:

$$S = \frac{\Delta\lambda}{\Delta n}(nm/RIU) \tag{9}$$

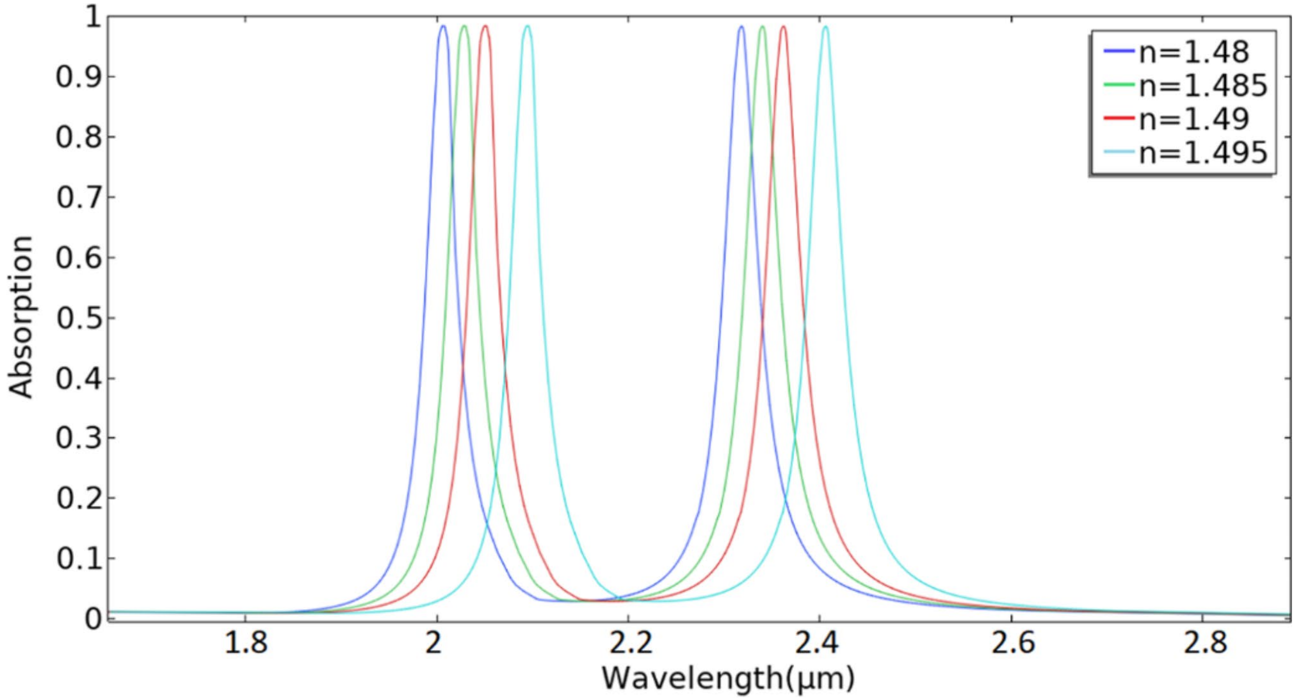

Fig. 12. Absorption spectrum vs. wavelength for different cholesterol concentrations.

References	Sensitivity (nm/RIU)	FOM (RIU^{-1})	Q-factor	LOD (RIU)
cholesterol sensor[55]	156.18	10.41		
cholesterol sensor[4]	2666.6	177.77		
cholesterol sensor[56]	245.6714			
cholesterol sensor[5]	5333.3	231.33	32.8	2.34e-4
cholesterol sensor[57]	1251			0.001
cholesterol sensor[58]	595.74		35–46	6.1e-3–6.7e-3
Our proposed cholesterol sensor	6045.6	237.61	80.3–90.1	2.1e-4–2.26e-5

Table 2. Comparison of our proposed sensor with previous works.

Another important parameter, figure of merit (FOM) can be calculated according to:

$$FOM = \frac{S}{FWHM}(RIU)^{-1} \tag{10}$$

In which, S and $FWHM$ stand for the sensitivity factor and full-width-at-half-maximum, respectively. The third important parameter is the Q-factor (quality-factor), which can be obtained according to[34,53]:

$$S = \frac{\Delta\lambda}{\Delta n}(nm/RIU) \tag{11}$$

where λ_{res} is the resonant wavelength (absorption's peak wavelength).

Last parameter is the limit of detection (LOD) which can be derived from[54]:

$$LOD = \lambda/(20 * S * Q) \tag{12}$$

For the presented biosensor, sensitivity factor, FOM, Q-Factor and LOD of 6045.6 nm/RIU, 237.61 RIU^{-1}, (80.3–90.1) and (2.1e-4–2.26e-5) RIU are obtained, respectively. Finally, the obtained results are compared with previously published works and are stated in Table 2.

Conclusion

In this work an efficient absorber based on plasmonic-graphene-black phosphorous configurations was presented and considered. The proposed device was based on quarter-cylindrical and plate shaped layers of graphene, black phosphorous, Ag, Au and Al_2O_3. The designed structure basically operated based on the PIT effect and was utilized for detection of cholesterol concentrations in blood samples (based on the obtained results physicians can diagnose hypercholesterolemia and prevent cardiovascular diseases or treat them in early stages). The improvement process of the absorption spectrum was conducted by considering the effects of structural parameters and chemical potential (E_f). Finally, various concentrations of cholesterol in blood samples were detected and sensitivity, FOM, Q-factor and LOD of 6045.6 nm/RIU, 237.61 RIU^{-1}, (80.3–90.1) and (2.1e-4–2.26e-5) RIU were obtained, respectively.

Data availability

All data generated or analyzed during this study are included in this published article.

Received: 31 January 2024; Accepted: 21 October 2024
Published online: 28 October 2024

References

1. Zheng, W. et al. An in-fiber sensor for simultaneous measurement of cholesterol concentration and temperature based on SPR and MMI. *Anal. Chim. Acta*. **1287**, 342043 (2024).
2. Cao, M. et al. Molecularly imprinted sensor based on cascade enzyme system supported by metal-organic framework (UiO-66-NH2) for sensitive colorimetric detection of cholesterol. *Sens. Actuators B*. **404**, 135235 (2024).
3. Ahmadi Arpanahi, R. et al. Coronary artery lipid accumulation prevention through vibrating piezo electric nano plates embedded in smart stent. *Med. Eng. Phys.* **118**, 104021 (2023).
4. Negahdari, R. et al. Sensitive biosensors based on plasmonic–graphene nanocombinations for detection of biological elements in blood samples. *Plasmonics*. **18**, 909–919 (2023).
5. Negahdari, R. et al. Sensitive MIM plasmonic biosensors for detection of hemoglobin, creatinine and cholesterol concentrations. *Diam. Relat. Mater.* **136**, 110029 (2023).
6. Fenghong, C. et al. Cholesterol biosensing based on hydrogel optical fiber immobilization with cholesterol oxidase. *Optik*. **286**, 170995 (2023).
7. Ding, L. et al. Dual-mode cholesterol sensor based on gold nanorods and carbon quantum dots. *Mater. Chem. Phys.* **309**, 128336 (2023).
8. Dasand, S. & Singh, V. K. Highly sensitive PCF based plasmonic biosensor for hemoglobin concentration detection, Photonics Nanostructures: Fundam. Appl 101040. (2022).
9. Chahkoutahi, A., Emami, F. & Rafiee, E. Sensitive hemoglobin concentration Sensor based on Graphene-Plasmonic Nano-structures. *Plasmonics*. **17**, 423–431 (2022).
10. Uniyal, A. et al. Recent advances in optical biosensors for sensing applications: A review. *Plasmonics*. **18**, 735–750. https://doi.org/10.1007/s11468-023-01803-2 (2023).
11. Daher, M. G. Supersensitive biosensor based on a photonic crystal nanostructure for blood sugar level monitoring with ultra-high quality factor and low detection limit. *Optik*. **275**, 170581 (2023).
12. Karki, B. et al. Tuning sensitivity of bimetallic, MXene and graphene-based SPR biosensors for rapid malaria detection: a numerical approach. *J. Comput. Electron.* **23**, 920–929. https://doi.org/10.1007/s10825-024-02191-4 (2024).
13. Daher, M. G. et al. Detection of basal Cancer cells using Photodetector based on a Novel Surface Plasmon Resonance Nanostructure employing Perovskite Layer with an Ultra High Sensitivity. *Plasmonics*. **17**, 2365–2373. https://doi.org/10.1007/s11468-022-01727-3 (2022).
14. Daher, M. G. et al. Highly sensitive detection of infected red blood cells (IRBCs) with plasmodium falciparum using surface plasmon resonance (SPR) nanostructure. *Opt. Quant. Electron.* **55**, 199. https://doi.org/10.1007/s11082-022-04466-1 (2023).
15. Rafiee, E., Negahdari, R. & Emami, F. Plasmonic multichannel filter based on split ring resonators: application to photothermal therapy. *Photonics Nanostructures: Fundam Appl.* **33**, 21–28 (2019).
16. Hajati, Y. Tunable broadband multi resonance graphene terahertz sensor. *Opt. Mat.* **101**, 109725. https://doi.org/10.1016/j.optmat.2020.109725 (2020).
17. Ghaedi, M. *Photocatalysis: Fundamental Processes and Applications* (Interface Science and Technology, 2021).
18. Deng, L., Liu, Z. & Li, L. Hybrid nanocomposites for imaging-guided synergistic theranostics. *Nanomaterials Drug Delivery Therapy*, 117–147. (2019).
19. Gholami, A., Shirkani, H., Sadeghi, Z. & Mehrabi, M. Designing a perfect phosphorene-Plasmon absorber and investigating its geometric irregularity effects: a simulation study, opt. *Laser Technol.* **156**, 108519 (2022).
20. Luo, P. et al. Dynamical manipulation of a dual-polarization plasmon-induced transparency employing an anisotropic graphene-black phosphorus heterostructure. *Opt. Express*. **29**(19), 29690–29703 (2021).
21. Wang, X. & Shi, Y. Fabrication Techniques of Graphene Nanostructures. Nanofabrication and its application in renewable energy, 1–30 DOI: (2014). https://doi.org/10.1039/9781782623380-00001
22. Bonaccorso, F. et al. Production and processing of graphene and 2d crystals. *Mater. Today*. **15**, 564–589 (2012).
23. Kasani, S., Curtin, K. & Wu, N. A review of 2D and 3D plasmonic nanostructure array patterns: fabrication, light management and sensing applications. *Nanophotonics*. **8**, 2065–2089. https://doi.org/10.1515/nanoph-2019-0158 (2019).
24. Zhang, Z. et al. Plasmonic sensors based on graphene and graphene hybrid materials. *Nano Convergence*. **9** https://doi.org/10.1186/s40580-022-00319-5 (2022).
25. Chau, Y. F., Yeh, H. H. & Tsai, D. P. Surface plasmon effects excitation from three-pair arrays of silver-shell nano cylinders. *J. Plasma Phys.* **16**, 022303 (2009).
26. Ho, Y. Z. et al. Tunable plasmonic resonance arising from broken-symmetric silver nano beads with dielectric cores. *J. Opt.* **14**, 114010 (2012).
27. Chau, Y. F. Surface Plasmon effects Excited by the Dielectric Hole in a silver-Shell Nano spherical pair. *Plasmonics*. **4**, 253–259 (2009).
28. Pal, A. et al. Tuning sensitivity of surface plasmon resonance sensor based on ZnO layer and CaF2 prism for the recognition of SARS-CoV-2. *J. Mater. Sci: Mater. Electron.* **35**, 1523. https://doi.org/10.1007/s10854-024-13287-9 (2024).
29. Li, M. et al. Dual-frequency on-off modulation and slow light analysis based on dual plasmon-induced transparency in terahertz patterned graphene metamaterial. *New. J. Phys.* **22**(10), 103030 (2020).
30. Zhang, X. et al. Photoelectric switch and triple-mode frequency modulator based on dual-PIT in the multilayer patterned graphene metamaterial. *J. Opt. Soc. Am. A*. **37**(6), 1002–1007 (2020).
31. Chen, S. et al. Multiple plasmon-induced transparency based on black phosphorus and graphene for high-sensitivity refractive index sensing. *Opt. Express*. **30**(24), 44004–44017 (2022).
32. Xiao, G. et al. Tunable and anisotropic perfect absorber using graphene-black phosphorus nanoblock, optics express. **30**(13), 23198–23207 (2022).
33. Mashayekhi, M. Z. et al. Dynamical controllable optical device designed by tunable graphene nanostructures in a PIT structure. *Optik*. **288**, 171185 (2023).

34. Rafiee, E. et al. An efficient biosensor based on plasmon-induced transparency effect in plasmonic-graphene-black phosphorous absorber for diabetes diagnosis. *Diam. Relat. Mater.* **140**(B), 110526 (2023).
35. Jia, Z. P., Huang, L., Su, J. B. & Tang, B. Tunable plasmon-induced transparency based on monolayer black phosphorus by bright-dark mode coupling. *Appl. Phys. Express.* **13**(7), 072006 (2020).
36. Han, L., Wang, L., Xing, H. Z. & Chen, X. S. Active control of plasmon-induced transparency with large tunability and high Q-factor in graphene-black phosphorus hybrid system. *J. Phys. D: Appl. Phys.* **54**(22), 225103 (2021).
37. Wang, X. J. et al. Hybrid metal graphene-based tunable Plasmon-Induced transparency in Terahertz Metasurface. *Nanomaterials.* **9**(3), 385 (2019).
38. Guo, X. et al. A tunable graphene-based dual PIT device with dual-polarization excitation capability. *Diam. Relat. Mater.* **141**, 110643 (2024).
39. Cai, Y. J. et al. Investigation of multi-resonant and anisotropic plasmonic resonances in the stacked graphene-black phosphorus bilayers. *J. Phys. D: Appl. Phys.* **53**(2), 025107 (2020).
40. Zheng, W. et al. A plug-and-play optical fiber SPR sensor for simultaneous measurement of glucose and cholesterol concentrations. *Biosens. Bioelectron.* **198**, 113798 (2022).
41. Feng, D. et al. Novel photoelectrochemical sensor for cholesterol based on CH3NH3PbBr3 perovskite /TiO2 inverse opal heterojunction coated with molecularly imprinted polymers, Sens. *Actuators B Chem.* **368**, 132121 (2022).
42. Liu, X. et al. A detection system for serum cholesterol based on the fluorescence color detection of beta-cyclodextrin-capped gold nanoclusters. *Spectrochim. Acta Part A Mol. Biomol. Spectrosc.* **308**, 123769 (2024).
43. Rahman, M. M. et al. Photonic crystal fiber based terahertz sensor for cholesterol detection in human blood and liquid foodstuffs. *Sens. Bio-Sens Res.* **29**, 100356 (2020).
44. Kumar, A. et al. Ultrahigh sensitive graphene oxide/conducting polymer composite based biosensor for cholesterol and bilirubin detection. *Biosens. Bioelectron. : X.* **13**, 100290 (2023).
45. Sahraeian, S. et al. Tunable Terahertz Absorber based on Graphene-Metal Nanostructure as opto-fluid Sensor. *Optik.* **242**, 166713 (2021).
46. Li, H., Niu, J. & Wang, G. Dual-band, polarization-insensitive metamaterial perfect absorber based on monolayer graphene in the mid-infrared range. *Res. Phys.* **13**, 102313 (2019).
47. Hanson, G. W. Dyadic Green's Functions and Guided Surface Waves for a Surface Conductivity Model of Graphene. *J. Appl. Phys.* **103** https://doi.org/10.1063/1.2891452 (2008).
48. Negahdari, R., Rafiee, E. & Emami, F. Design and simulation of a novel nano-plasmonic split-ring resonator filter. *J. Electromagn. Waves Appl.* **32**, 1925–1938 (2018).
49. Wu, K. et al. Slow-light analysis based on tunable plasmon-induced transparency in patterned black phosphorus metamaterial. *J. Opt. Soc. Am. A*. **38**(3), 412–418 (2021).
50. Xiong, C. X. et al. Triple plasmon-induced transparency and outstanding slow-light in quasi-continuous monolayer graphene structure. *Sci. China Phys. Mech. Astron.* **64**(2), 224211 (2021).
51. Rafiee, E. & Emami, F. Investigating the effects of structural parameters on the optical characteristics of add-drop filters. *Optik.* **127**, 1690–1694 (2016).
52. Jin, Y. L., Chen, J. Y., Xu, L. & Wang, P. N. Refractive index measurement for biomaterial samples by total internal reflection. *Phys. Med. Biol.* **51**, 371–379. https://doi.org/10.1088/0031-9155/51/20/N02 (2006).
53. Chorsi, H. T. et al. Tunable plasmonic substrates with ultrahigh Q-factor resonances. *Sci. Rep.* **7**, 15985 (2017).
54. White, I. M. & Fan, X. On the performance quantification of resonant refractive index sensors. *Opt. Express.* **16**, 1020–1028 (2008).
55. Lu, Y. et al. Beta-cyclodextrin based reflective fiber-optic SPR sensor for highly-sensitive detection of cholesterol concentration. *Opt. Fiber Technol.* **56**, 102187. https://doi.org/10.1016/j.yofte.2020.102187 (2020).
56. Fu, X. et al. High sensitivity refractive index sensor based on cascaded core-offset splicing NCF-HCF-NCF structure, opt. *Fiber Technol.* **68**, 102791 (2022).
57. Hou, Z. et al. Highly sensitive cholesterol concentration trace detection based on a microfiber optic-biosensor enhanced specificity with beta-cyclodextrin film. *Spectrochim Acta Mol. Biomol. Spectrosc.* **300** (122881).
58. Rafiee, E. et al. Hypercholesterolemia diagnosis by a biosensor based on photonic crystal PANDA structure. *Opt. Rev.* **31**, 87–93. https://doi.org/10.1007/s10043-023-00859-z (2024).

Author contributions
Esmat Rafiee contributed to the study conception and design. Material preparation, data collection and analysis were performed by Esmat Rafiee. The manuscript was written by Esmat Rafiee.

Funding
The authors declare that no funds, grants, or other support were received during the preparation of this manuscript.

Declarations

Competing interests
The authors declare no competing interests.

Additional information
Correspondence and requests for materials should be addressed to E.R.

Reprints and permissions information is available at www.nature.com/reprints.

Publisher's note Springer Nature remains neutral with regard to jurisdictional claims in published maps and institutional affiliations.